Thermal Scalar Field for Continuous three-dimensional Toolpath strategy using Wire Arc Additive Manufacturing for free-form thin parts

A Giordano, A Diourté, C Bordreuil, Florian Bugarin, S Segonds

Thermal Scalar Field for Continuous Three-dimensional Toolpath Strategy Using Wire Arc Additive Manufacturing for Free-form Thin Parts

A. Giordano [a,*], A. Diourté [a,b], C. Bordreuil [c], F. Bugarin [a], S. Segonds [a]

[a] Institut Clément Ader (ICA), Université de Toulouse, UT3, CNRS, IMT Mines Albi, INSA Toulouse, ISAE-SUPAERO, Toulouse, France
[b] Avantis Project, Aéroparc, 12 Rue de Caulet, 31300 Toulouse, France
[c] Laboratoire de Mécanique et de Génie Civil, Université de Montpellier / CNRS, Montpellier, France

A B S T R A C T

Wire Arc Additive Manufacturing (WAAM) is revolutionizing the field of Additive Manufacturing (AM) by being the technological solution to manufacture thin-walled structures of large dimensions and medium geometric complexity at reduced cost with an excellent buy-to-fly ratio. Manufacturing parts with this technology is nowadays done through 2.5D strategies. This type of strategy consists in cutting a 3D model using planar layers parallel to each other. This 2.5D technique limits the complexity of the geometries that can be produced in WAAM without taking advantage of height deposit modulation. It also requires several start/stop phases of the arc during the transition from one layer to another, which leads to poor quality. This paper presents a new fast and efficient path planning strategy aiming at creating a continuous manufacturing path, thus increasing poor part quality. This strategy so called "Scalar Thermal Field for Continuous Toolpath" is generating a continuous spiral manufacturing toolpath for thin shaped parts. The modulation of deposition, by controlling the welding torch travel speed at constant wire feed rate, allows continuous deposition of material throughout the manufacturing process. The keypoint of the method is the use of a thermal scalar field associated with a 6-axis robotic arm kinematics which allows the manufacturing of closed parts after optimal closure point determination or direct manufacturing of opened parts with non-planar free edges. Validation of the presented method is performed by manufacturing three distinct parts : an opened, a closed part and a multi-branch part. The fabrication of these parts and their precise measurement have shown the reliability and the restitution capacity of our method which is clearly superior to 2.5D strategies nowadays commonly used in WAAM technology.

Keywords:
Wire Arc Additive Manufacturing (WAAM)
Continuous three-dimensional (3D)
toolpath
5-axis strategy
Thermal scalar field
Free-form thin parts

1. Introduction

Wire Arc Additive Manufacturing (WAAM) is revolutionizing the field of Additive Manufacturing (AM) by being the technological solution for manufacturing thin-walled structures of large dimensions and medium geometric complexity at reduced cost [1]. For more details on WAAM, the reader can refer to the article [2]. Because of its buy-to-fly ratio, it is a very attractive technology in the aeronautics industry [3]. WAAM could be applied to many other fields such as aeronautics parts repairing or functionalities addition. WAAM is also very well adapted for topologically optimized parts which are often hollow shelled parts which can hardly be obtained using conventional manufacturing process. It is also possible to use WAAM to manufacture parts and to perform a post-fabrication phase in order to obtain the desired precision in the so-called "working" areas (local machining of mounting surfaces for example). Due to technical considerations inherent to its technology, the promising attractions of WAAM do not yet allow its wide use in the industrial world. These include residual stresses related to melt cooling, distortion and manufacturing strategy [4]. Ding et al. [5] have shown that the manufacturing strategy is closely related to the quality of the manufactured part by acting on the material deposition. 2.5D deposition strategy which is very well adopted for plastic part 3D printing as in Fused Deposition Modeling (FDM), is also commonly used in WAAM. However 2.5D strategy generates a poor part quality due to the multiplication of start/stop phases. These phases generate important defects on the quality of the surface finish and imply cooling times before initiating a new bead which leads to a longer manufacturing time. The implementation of a

* Corresponding author.
E-mail addresses: arthur.giordano@univ-tse3.fr (A. Giordano), adama.diourte@univ-tlse3.fr (A. Diourté), cyril.bordreuil@umontpellier.fr (C. Bordreuil), florian.bugarin@univ-tlse3.fr (F. Bugarin), stephane.segonds@univ-tlse3.fr (S. Segonds).

generic and fast manufacturing strategy is thus necessary to be competitive with 2.5D strategies. In this paper, a new method for 3D deposition using thickness variation along the manufacturing is presented. This variation is based on an assumption of thickness variation of the shell. Indeed, the bead is modeled as cylindrical and its radius varies linearly according to the material input and the welding nozzle feed rate. This strategy is based on an easy to complete heat scalar field which will be used for rapidly determining a continuous optimal toolpath while limiting thickness deposit variation. This method is very versatile by adapting to all types of geometry. Diourte et al. [6] have implemented a 3D continuous trajectory generation method that discretizes a part using generators. The difference between these two methods lies in the fact that the present method allows a much faster and easier segmentation of the part than the one previously mentioned. Also the present method does not require any additional operations depending on the part to be manufactured.

1.1. Related works

WAAM technology is a fairly recent technology that is currently limited by the complexity of the parts to be manufactured. Indeed, in Additive Manufacturing (AM), most of the strategies used are in 2.5D. This method of trajectory generation consists in the cutting a CAD model into three-dimensional layers according to the direction of construction, which is perpendicular to their mean plane. These layers can have a constant spacing between them, called uniform slicing, or a variable spacing, called adaptive slicing. The adaptive slicing realized by Ma et al. [7], allows to automatically adjust the inter-layer distance by improving the geometry restitution. The 2.5D strategies use different filling techniques of the 2D layers resulting from the geometry cutting. We can find patterns such as rasters, spirals, zigzags [8,9]. This type of strategy is well suited for powder-based technologies such as Selective Laser Sintering (SLS) or Fused Deposition Modeling (FDM). Ivan Sosin et al. [10] proposed an algorithm to build lattice structures via sphere stacking while respecting the geometry. This method allows to process solid or semi-solid parts while optimizing the BTF ratio. One of the interests of WAAM is its high deposition speed, which is significantly higher than powder-based technology and therefore must be adapted accordingly. It also allows a modulation of the deposition height, which is interesting in a three dimensional strategy. However, this parameter must be controlled precisely because it is greatly impacted by the start and stop phases of the arc which number has to be as small as possible. According to Zhang et al. [11], the height of the bead is higher at the beginning than at the center of the bead and is lower at the end of the bead. This phenomenon causes problems with the deposition height, which is amplified in the following layers by increasing the difference between the beginning and the end of the bead [11], which does not give the expected final geometry or produce collision between torch and part if part geometry is not monitored. To solve this problem of height uncontrolled variations between different successive layers, Ding et al. [12] proposed the idea that continuous deposition should be performed in a closed loop by minimizing start/stop phases of the arc. A control of the weld bead geometry has been proposed by Kwak et al. [13] to limit the height differences between layers. Wang et al. [14] developed a method to monitor and control the width and reinforcement of the weld bead online, layer by layer. In order to control the size of the melt, Montevecchi et al. [15] decided to introduce idle times to allow the cooling down of the part being manufactured. With this type of planning, it seems to be possible to maintain a constant bead size throughout the manufacture of the geometry. However, these strategies have been tested on simple parts with simple geometries and their extension to complex thin parts has not been studied yet. The manufacturing trajectories may present discontinuities such as angles and overlaps influencing the quality of the deposit and impacting the quality of the part manufactured. Several studies focusing on these problems already exist, evoking the idea of path planning [5,7,8] allowing to increase the quality of large size parts with 2.5D strategies applied to WAAM. Different methods have been developed to realize parts described using mathematical equations [16,17] with closed structures. These solutions need specific strategies depending on the geometry and are therefore not generic. The rise of AM technologies has allowed the development of 2.5D path planning strategies taking into account the constraints associated with the process. These methods limit the range of complexity of the structures that can be produced because of the use of 3-axis machines. The parts manufactured with these strategies have a poor surface finish. In addition, they are subject to staircase effect that generates a poor geometric precision due to the planar cutting. In order to reduce this staircase effect, it is possible to reduce the deposition height as with powder-based technologies. Polymer-based AM, in addition to reducing the deposition height to limit this undesirable effect, can use a curvilinear cutting technique unlike 2.5D strategies such as the CurviSlicer [18]. However, these methods are not suitable for WAAM which has a too high deposition rate that makes difficult the important reduction of height deposition. Moreover, the 2.5D strategies are based on the use of 5 axis, but do not use the full potential of this kind of material by using only 3 axes. It has been shown by Hascoët et al. [19] that the use of 5 axes is necessary for the fabrication of inclined structures or structures with curvature variations. The advantage of using 5-axis is that it allows the tilting of the nozzle. This freedom of movement also makes it possible to get rid of supports which are not interesting with the WAAM, since their manufacturing is time consuming. Ezair et al. [20] have developed a method to optimize the angle of the fabrication direction to limit the need for supports. For lattice structures, we find in the literature algorithms allowing to avoid manufacturing support by making self-supporting lattice parts [21]. The decomposition of the part to be manufactured greatly facilitates its manufacture when collisions between the part and the welding torch are taken into account while guaranteeing a self-supporting part thanks to a lattice structure or with a segmentation in convex curved layers [22,23]. Wu et al. [24] developed a 3D printing algorithm to overcome the need for a support structure by using a segmentation method to cut a geometry into self-supporting elements. The generation of curved layers proposed by Fang et al. [25] allows to create an optimized toolpath according to the main stress directions, which allows a gain of mechanical performance on the manufactured part. Indeed, with a use on 3 axes, the nozzle can always remain perpendicular to the layer to be deposited contrary to a 5 axis strategy where the nozzle remains tangential to the surface of the part to be manufactured. The main interest of this technique is to increase the quality of the manufacturing part by eliminating the staircase effect [19]. A continuous path also saves manufacturing time. Indeed, it has the effect of limiting the start/stop phases of the arc, which are very time-consuming. These phases, as presented in the Montevecchi study [15], introduce inactivity times that directly impact the productivity. Hergel et al. [26] propose a strictly continuous clay manufacturing trajectory that is possible due to the use of support in order to move from one layer to another. However, WAAM does not allow for easy removal of the support and this would increase the BTF ratio which is one of the major advantages of this technology. Iso-curve extraction algorithms from scalar fields have been developed to convert them into spiral paths [27,28]. Xu et al. [29] developed a method to create a continuous trajectory using iso-contours

extracted from geodesic distances. This method can handle closed parts and opened parts with an upper free edge perpendicular to the manufacturing direction but is limited on parts with a non-planar upper free edge. Diourte et al. [6] have proposed a 3D continuous trajectory strategy based on geodesic distance calculation. This method requires a high computation time and geometries with singularities or flared shapes must go through a generator creation step in order to create the continuous trajectory. In order to take advantage of WAAM, to increase the complexity of the manufactured geometries while keeping a good rendering accuracy, a new strategy of trajectory generation with a different approach from the 2.5D and using the 5 axes proposed by the tools has to be set up. This method will also have to be fast to compete with 2.5D methods.

1.2. Contributions

In this paper, a fast 3-dimensional continuous path planning strategy using a scalar field based on heat propagation is presented. This method is declined for thin parts of free-form shapes of three types : opened, closed and multi-branch which are an extension of the opened and closed geometries. This continuous path generation strategy allows to limit the start/stops phases of the weld bead required for the fabrication of structures with the WAAM process. Moreover, one of the advantages of this manufacturing process is the modulation of the height of the material deposit, contrary to powder bed-based technologies. This modulation is constrained in a range $[h_{min}, h_{max}]$ where h_{min} is the minimum deposition height and h_{max} is the maximum. This variation in deposition height depends on the different control parameters WAAM. This strategy combining the use of a 6-axis robotic arm and deposition modulation allows the manufacturing of various shapes using WAAM, such as closed parts with minimal start/stop phases of the arc or parts with non-planar free edges thanks to the curved paths (Fig. 1). The presented method is based on the use of a scalar field with Dirichlet boundary conditions to quickly extract iso values that will be used to generate the WAAM manufacturing path of the studied parts. Start/stop phases are minimized and bead thickness is chosen as constant as possible. In the context of this work, a robotic arm 6 axes with a welding torch are used. This robot has 6 degrees of freedom including 3 translations (X, Y, Z) and 3 rotations (Rx, Ry, Rz) linked to a Cartesian coordinate system [30]. The wire feeding speed and the welding speed are controlled in real time to modulate the deposit height at any moment of the manufacturing process. Structures with non-planar boundary surfaces, such as Fig. 1(a), are manufactured for validation of the method on parts with curved surfaces, such as pipes. Non-planar boundary surfaces manufacturing makes possible the adding of functionalities to already existing structures [12,31] thus extending the possible use of the presented strategy. This makes it possible to create opened and closed free-form parts without interrupting the weld bead and saves manufacturing time on strategies that require interruptions of the weld bead while guaranteeing a better part quality. This strategy can be split into two parts depending on the topology of the part:

- Opened parts which are defined by geometric shapes with a free edge in addition to the one in contact with the substrate (Fig. 1(a)).
- Closed parts which are defined by geometrical shapes having only one free edge in contact with the substrate (Fig. 1(b)).

Opened multi-branch (Fig. 1(c)) and closed multi-branch parts which are defined by geometrical shapes with several branches like a tree. A segmentation algorithm for these multi-branch parts has been implemented in order to be able to split them into simple elements and to apply the same method as for opened or closed parts in order to generate a continuous toolpath.

The purpose of this paper is to present a continuous spiral toolpath generation method for thin opened or closed parts with planar and non-planar free edges, called Thermal Scalar Field for Continuous Trajectory. A scalar field will be used, with Dirichlet boundary conditions, in order to allow the extraction of iso-values on all types of geometries. This scalar field called "thermal" is detailed in Section 2.1. The geodesic distances do not allow the correct treatment of opened geometries, such as the geometry called "Elephant's trunk" which is treated in the article because of its non-planar upper free edge. A comparison between the geodesic and thermal scalar field is presented on an opened part in Section 3.1 in order to show the versatility of the thermal scalar field compared to geodesic distances. The toolpath created with our method guarantees the modulation of the deposition height in the interval $[h_{min}, h_{max}]$ related to the tooling used and defined by the end user.

This paper is organized as follows. In Section 2, we introduce the idea of a thermal scalar field constrained by the free edge and describe how to construct 3D curves from this field in order to generate the toolpath. Then, in Section 3, we present the application of toolpath generation on three models of distinct geometries. Section 4 presents the fabrication and validation of our method by manufacturing three parts with different shape constraints, followed by the conclusion in Section 5.

2. Thermal Scalar Field for Continuous Toolpath

In Thermal Scalar Field for Continuous Toolpath, the part is first modeled with CAD software as in all AM strategies. After this first step, the average geometry is converted to an STL file. The STL file will be the one of the nominal model of null thickness. The real part will be tick and we will observe a part thickness relative to this neutral fiber of more or less half the average deposit height. This file format represents the shape of the part as a triangular mesh where each triangle is described as a facet by three vertices with their own coordinates that compose a unit vector representing the normal to each facet. The mesh of the parts must be uniform, which means that the three edges must have a similar size to avoid having elongated triangular meshes. Elongated triangles have to be avoided for the calculations, as they can lead to inaccurate information. The STL format allows the use of the various algorithms that are necessary for the continuous toolpath strategy. The type of geometry that can be manufactured is described in the following Section 2 and the strategy itself in the following Section 2.2–2.4. Single and multi-branch parts can have two types of geometries, opened and closed, so our strategy adopts two concepts. In the first part, the methodology on opened parts is exposed and the second part is devoted to closed parts. It is important to separate these two parts, because the needs of these two types of geometries are not the same and therefore neither is the strategy. A third type of parts has been studied in order to make this method more versatile, these are the so-called multi-branch parts and a last strategy has been developed to meet the constraints inherent to these geometries.

2.1. Decomposition by iso-values

The idea of our method is to map a geometry to be fabricated using a 3D scalar field between the bottom and the top of the latter in order to decompose it into a series of 3D level lines corresponding to iso-contours which could also be called iso-temperatures. The scalar field will be called "thermal scalar field" in reference to the classical use of this type of scalar field to evaluate temperatures in continuum, in permanent regime for a pure conduction phenomenon. We have therefore assumed that

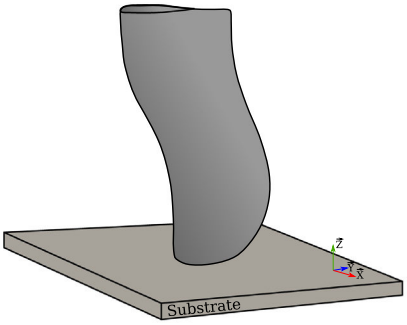

(a) Opened part called "Elephant's trunk".

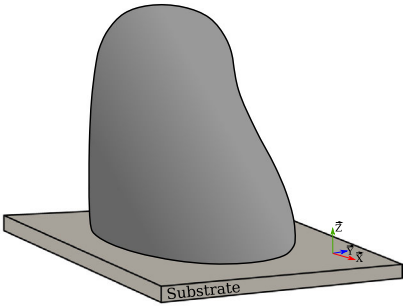

(b) Closed part called "Elephant's foot".

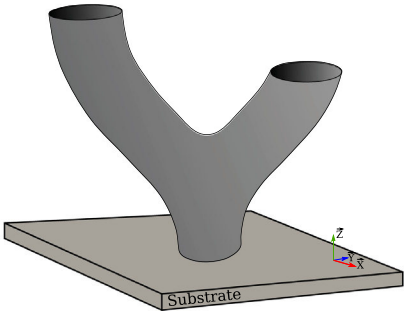

(c) Non-symmetrical multi-branch part.

Fig. 1. Opened part with non-planar boundary, closed part and non-symmetrical multi-branch part.

there is no convection nor radiation. This scalar field is computed with a finite element code [32] under PYTHON allowing to solve the heat equation (Eq. (1)), with Dirichlet conditions on the edges of the domain such that $T_{lower} \neq T_{upper}$. The solution of the equation is done in a linear way to reduce the computation time on large parts or with a "fine" mesh which is derived from the STL file used as input. In the following, we will use the term thermal scalar field to refer to the scalar field described above.

$$\Delta u = 0 \tag{1}$$

In our study, we have chosen to take T_{lower} lower than T_{upper} and that the latter are sufficiently different. In order to apply the boundary conditions, it is necessary to determine where to apply them. The lower boundary condition value is applied at the lower free edge, in contact with the substrate and the upper one is applied at the upper free edge. Depending on the type of geometry, the upper free edge may not exist (Fig. 1(b)), so it is first necessary to determine it. Geodesic distances will be calculated and used for closed parts as detailed in Section 2.3. Heat propagation is initiated between the two free edges and a numerical value is given at each point of the Ω domain. Thanks to the computation of this scalar field on the geometries, it is possible to create n_{layers} iso-contour lines $S = \{S_1, \ldots, S_{n_{layers}}\}$.

Fig. 2 illustrates the creation of iso-contours using the thermal gradient applied to the mesh. Each node in the mesh has a temperature value that allows the creation of level lines based on the number of iso-values required. The creation of an iso-contour is the result of an interpolation between two nodes, as can be seen in Fig. 2, where, for example, the iso-contour S_i is the level line with a value of 33 following the number of layers. The number of layers depends on the minimum height h_{min} of the modulation range of material deposition by the weld bead which is detailed in Section 2.5. The level lines are connected one by one to generate the 3D continuous toolpath as explained in Section 2.6.

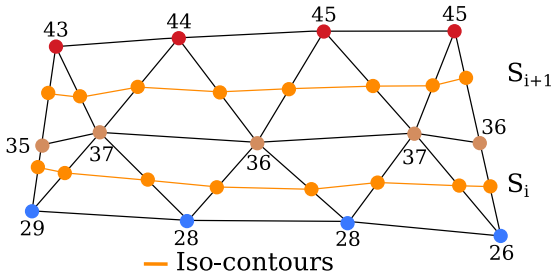

Fig. 2. Method of generating the iso-contours by interpolating the information at the nodes of the mesh.

The use of the scalar field allows the extraction of iso-contours on all types of geometries. The use of geodesic distances does not allow to treat correctly opened geometries, like the geometry called "Elephant's trunk" which is treated in the paper because of its non-planar upper free edge. A comparison between the geodesic and thermal scalar field is presented on an opened part in Section 3.1 in order to show the versatility of the thermal scalar field in contrast to geodesic distances.

2.2. Opened parts

Opened parts are composed of two free edges, one free edge $\partial\Omega_{lower}$ in contact with the substrate and one at the top of the geometry $\partial\Omega_{upper}$ as represented in Fig. 3. This particularity of these shapes does not require any operation prior to the application of the method unlike for closed part as presented in the following section. The first step of this method consists in imposing an initial temperature T_{lower} to the n_{lNodes} nodes belonging to the lower free edge $\partial\Omega_{lower}$ noted Pi_{lower} with $i \in [1, n_{lNodes}]$ and a final temperature T_{upper} assigned n_{uNodes} points belonging to the upper free edge $\partial\Omega_{upper}$ noted Pj_{upper} with $j \in [1, n_{uNodes}]$. The temperature difference between the two free edges will create

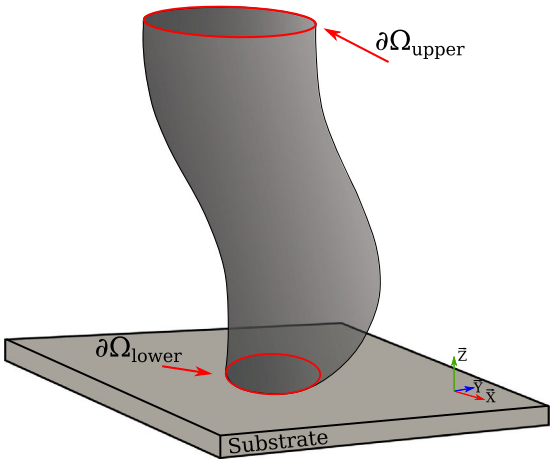

Fig. 3. Free edge $\partial\Omega_{upper}$ at the top and in contact with the substrate $\partial\Omega_{lower}$ of opened part.

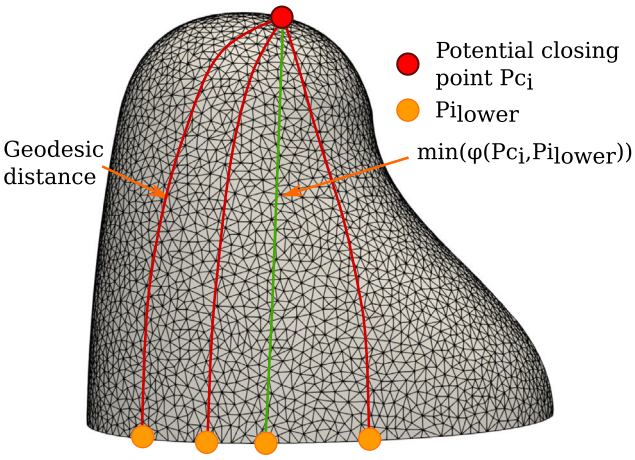

Fig. 4. Search for the optimal closing point on "Elephant's foot" part.

a temperature spread over the entire surface of the geometry. Each vertex of the Ω mesh is assigned a temperature information and allows to have a thermal mapping on the whole part. Thanks to this information, it is possible to create iso-temperature lines which is necessary to create the trajectory.

2.3. Closed parts

The closed parts are not provided with upper free edges, that is why it is necessary to determine the optimal closing zone $Zc_{optimal}$ and to use it thereafter as upper free edge $\partial\Omega_{upper}$. The manufacturing strategy is based on these two free edges, hence determining the closing zone and more precisely the optimal closing point $P_{optimal}$ to allow the manufacturing of these parts with a single weld bead by varying the deposition height in the range $[h_{min}, h_{max}]$ is crucial.

2.3.1. Optimal closing point

This optimal closure point $Pc_{optimal}$ can easily be found in a simple case like a half sphere where it is located at its vertex, because the geometry is axisymmetric. However, for any geometry, we need to determine this point in an efficient and optimal way. The main idea is to find a closing point minimizing the variation of weld bead thickness along the whole manufacturing process. To find this point, the notion of geodesic distance is used. The geodesic distance [33] is defined as the distance, denoted $\varphi(Pc_i, Pi_{lower})$, representing the shortest distance between two points Pc_i and Pi_{lower} based on the surface Ω (Fig. 6), where Pi_{lower} is a point belonging to the lower free edge and Pc_i is the optimal closure point. The geodesic distance can be written in the following form (Eq. (2)).

$$G = \varphi(Pc_i, Pi_{lower}) \tag{2}$$

The single free edge $\partial\Omega_{lower}$, in contact with the substrate, of the part is composed of the points Pi_{lower} which are the vertices of the mesh belonging to $\partial\Omega_{lower}$ that are used in the computation of the geodesic distances such as $G = \{G_1, \ldots, G_{n_{layers}}\} \in \partial\Omega_{lower}$.

For each of the n_{vertex} vertices of the Ω mesh of the closed part, the minimum geodesic distance is computed to the Pi_{lower} of the free edge $\partial\Omega_{lower}$ as presented in Fig. 4. The optimal closure point $P_{optimal}$ is therefore the point maximizing the geodesic distance computed previously, which can be written in this form with G defined in Eq. (2).

$$Pc_{optimal} = max(min_{P\in\Omega}(G)) \tag{3}$$

In order to reduce the computation time of the closing point position, it is possible to define a zone of the mesh and to test only the points located inside it. For example on the part (Fig. 4), it is possible to find this area intuitively, which is located at the top of the geometry. After having found the coordinates of the optimal closure point, the same process will be applied to the closed part as to the opened part. Indeed, the principle of heat propagation requires an upper free edge. In the case of the closed geometries, having no upper free edge, the final temperature T_{upper} is applied to the closed point $P_{optimal}$ and the initial temperature T_{lower} is applied to the n_{lNodes} nodes belonging to the lower free edge $\partial\Omega_{lower}$ noted Pi_{lower} with $i \in [1, n_{lNodes}]$ and the heat propagation will be as for opened parts.

2.4. Multi-branch parts

Multi-branch parts are an extension of the opened and closed parts presented in Sections 2.2–2.3. A multi-branch geometry can be defined by its skeleton. A skeleton is the result of reducing a shape into a set of curves centered in the original shape. We can quote several methods of skeletonization as distance transform field-based methods [34–36], Voronoi diagram-based methods [37,38], and thinning-based methods [39,40]. The method presented in [40] is used in the present work and allows to know if the geometry is considered as a multi-branch or not, with the separation of the skeleton into two branches (see Fig. 5).

The method will be applied with the same requirements for an opened (.resp closed) multi-branch part as for an opened (.resp closed) part. Multi-branch parts are composed of one or more free edges $\partial\Omega_{lower}$ in contact with the substrate and one or more at the top of the geometry $\partial\Omega_{upper}$ as represented in Fig. 5. In the case where the multi-branch part is a totally closed part, which therefore has no free top edges $\partial\Omega_{upper}$, we must therefore find the temporary optimal closure point in the part, see Section 2.3.1. Indeed, the segmentation of the closed multi-branch part will find the optimal closure point of each branch reduced to a simple trunk-like element. The path generation method is based on the idea of making continuous paths. It is very easy to obtain a continuous path with single-branch parts, but in the case of a multi-branch part, it is impossible to achieve a continuous path. In fact, it is only possible to manufacture a multi-branch part, branch by branch, by making a continuous path for each of its branches. As can be seen from the shapes in Fig. 1(c), we need $N + 1$ paths with N, the number of branches. The branch which could be similar to the trunk of a tree does not count in the number of branches. The analogy with trees has been used a lot

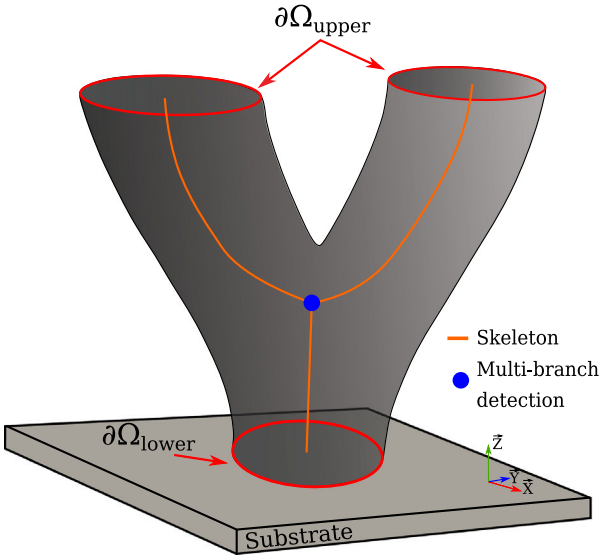

Fig. 5. Two Free edges $\partial\Omega_{upper}$ at the top and in contact with the substrate $\partial\Omega_{lower}$ of non-symmetrical multi-branch part.

in this work, as it is parallel that is often made in the literature. A method will be presented to segment the part in order to apply the toolpath generation algorithm on each of the branches independently, as on single-branch parts.

2.5. Calculation of the number of level layers

The calculation of the number of level layers is important to determinate the number of revolutions needed to manufacture the parts. Thus geodesic distance is used and its calculation method is slightly different according to the type of parts in the Sections 2.5.1–2.5.2. The notion of geodesic distance is previously described in Section 2.3.1.

2.5.1. Closed parts

The calculation of the number of layers for the closed part is easy to compute, because the geodesic distances G were already computed in Section 2.3.1. Indeed, in the above mentioned section, the geodesic distances have been computed to find the optimal closing point (Fig. 4).

2.5.2. Opened parts

For opened parts, the calculation of geodesic distances between upper and lower free edge have to be done. In this case, the lower free edge $\partial\Omega_{lower}$ which is composed of Pi_{lower} points that are the vertices of the mesh belonging to $\partial\Omega_{lower}$ are used as source points for the computation of the geodesic distances such as $G = \{G_1, \ldots, G_{n_{layers}}\} \in \partial\Omega_{lower}$. The target points for the calculation of geodesic distances are the n_{pts} points belonging to the upper free edge $\partial\Omega_{upper}$. For each target point, the minimum geodesic distance from the n_{pts} points of $\partial\Omega_{lower}$ must be calculated. An example of this calculation is illustrated with Figs. 6.

After the geodesic distances have been calculated, the number of layers n_{layers} is determined using Eq. (4). G_{layers} is the minimum geodesic distance to the bottom free edge $\partial\Omega_{lower}$ and h_{min} the lower bound of the deposition modulation interval.

$$n_{layers} = floor\left(\frac{min(G_{layers})}{h_{min}}\right) \tag{4}$$

2.6. Continuous path generation

In order to create a continuous spiral trajectory, a last step has to be done to smoothly go from a layer to the following one. Each iso-temperature is discretized in n_{pts} allowing the construction of the continuous trajectory by connecting the points one by one. To do this, the proper points of the trajectory noted $Z = \{Z_1, \ldots, Z_{n_{pts}}\}$ are created according to the following method. Let an iso-temperature S_1 and a second iso-temperature S_2 be such that the n_{pts} of the iso-temperature S_1 are noted $X = \{X_1, \ldots, X_{n_{pts}}\}$, respectively $Y = \{Y_1, \ldots, Y_{n_{pts}}\}$ those of S_2. The final points Z are created by following a linear distribution between the two iso-temperatures S_1 and S_2 is obtained the distribution of points given by Eq. (5) with $i \in [1, n_{pts}]$.

$$Z = \{Z_1, \ldots, Z_{n_{pts}}\} \tag{5}$$

where :

$$Z_1 = X_1 \times \frac{n_{pts} - 1}{n_{pts}} + Y_1 \times \frac{1}{n_{pts}}$$

$$Z_i = X_i \times \frac{n_{pts} - i}{n_{pts}} + Y_i \times \frac{i}{n_{pts}}$$

Following the distribution obtained in Eq. (5), is obtained a spiral trajectory between two iso-temperatures (Fig. 7). This pattern between all the iso-temperatures is repeated to obtain the continuous trajectory for final manufacturing.

2.7. Segmentation of multi-branch parts

In this section, the method for managing multi-branch parts will be explained in more detail thanks to the simple geometry used in Fig. 1(c). Segmenting a multi-branch geometry allows it to be decomposed into simple branch shapes that can be manufactured using a continuous path. This splitting into simple elements ensures that the feasibility criterion of Section 4.3 is satisfied within the deposition modulation range of the technology. As it can be seen in the algorithm 1, this method is based on the detection of a multi-branch. The detection of a multi-branch is the point where the skeleton splits in two, going from one branch to two branches as we can see in Fig. 5 in Section 2.4, or inversely. To split the multi-branch part, we use a principle of traversing the part in the direction of manufacture, from the base of the geometry to its top, in order to segment the latter. We summarize the entire multi-branch model segmentation process in detail below.

Algorithm 1: Multi-branch_Segmentation

```
function Multi-branch_Segmentation (Ω, h_min);
Input  : The geometry represented by its average surface
         mesh Ω and free edges ∂Ω.
Output: A toolpath for each branch.
vDetect, S_multi, S = ThermalScarlarField(Ω, h_min)
if vDetect == True then
    Ω_branch = branchExtractor(Ω, S_multi);
    vDetect, S_multi, S = ThermalScarlarField(Ω_branch, h_min);
    createToolPath(S);
else
    createToolPath(S);
end
```

- Application of the path generation method:

The path generation method is the basis of this segmentation method, to do this the temperature T_{lower} is assigned to the nodes of the lower free edge $\partial\Omega_{lower}$ and the temperature T_{upper} is assigned to all the nodes of the upper free edge $\partial\Omega_{upper}$, see

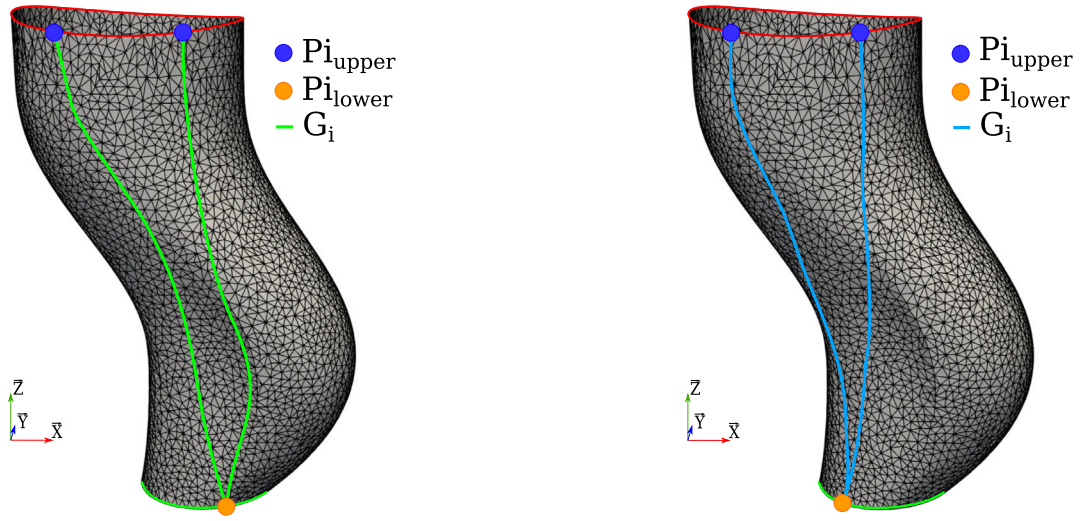

(a) Geodesic distances G_i on opened part.

(b) Geodesic distances G_i on opened part.

Fig. 6. Calculation of geodesic distances on the opened part to calculate the number of layers.

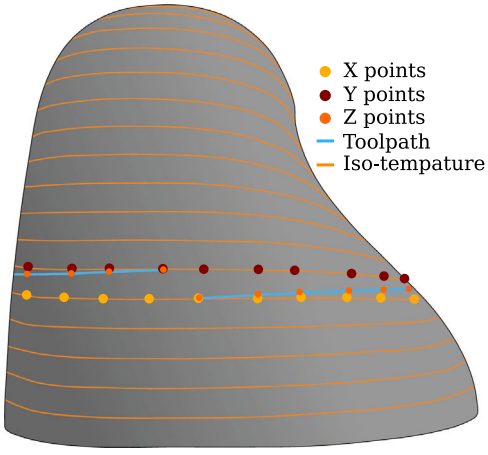

Fig. 7. Strategy for creating a continuous trajectory by connecting the points created from the points belonging to the iso-temperatures.

Fig. 5, so we find an identical temperature on the whole nodes of the upper free edge $\partial\Omega_{upper}$. However, in the case where the multi-branch part is a closed part, which does not have a free upper edge $\partial\Omega_{upper}$, it is therefore necessary to find a first optimal closure point, see Section 2.3.1. This closure point will allow us to apply the T_{upper} necessary for the path generation algorithm in order to obtain a mapping of the thermal scalar field on the whole part. Once this step is done, we must proceed to the extraction of the iso-temperatures which are essential to proceed to the segmentation of the geometry in simple elements. Indeed, the segmentation of the multi-branch part will allow to find the optimal closing point of each closed branch in order to apply again the trajectory generation method on this geometry and to compute its toolpath thereafter. Obtaining the thermal scalar field allows us to recover iso-temperatures which will be used to split the geometry. Now, we need to know where to cut the part and therefore know which iso-temperature to use.

- Detecting a multi-branch:

To detect multi-branch initiation on the geometry, the use of the skeleton could have been considered. However, the iso-temperatures have already been calculated previously, making the method faster to use. The iso-temperatures are simple contours so their interest is twofold, the creation of the trajectory and in this case the detection of a multi-branch. This detection will be done during the course of the iso-temperatures $S_{n_{layers}}$ from the bottom to the top in the direction of manufacture of the part. The multi-branch detection will be done when, during the course of the contours, the presence of an iso-temperature with two loops appears, which we will note S_{multi} as we can see in Fig. 8.

- Cutting the geometry and extracting the branches:

The part is split in two thanks to the iso-temperature S_{multi} through the VTK library [41]. The iso-temperature $S_{multi-1}$ visible in Fig. 8 allows to cut the lower branch and the iso-temperature S_{multi} allows to cut the upper part. We can notice that the shape cutting will leave a hole on the geometry, between the $S_{multi-1}$ contour and the S_{multi}. However, the deposition strategy will allow, thanks to the thickness of the weld bead, to fill this hole in the geometry and the fidelity between the CAD and the manufactured part will be respected. As for the upper part, it is necessary to extract the branches independently. To do this, we use the principle of connectivity of the triangles of the mesh. A triangle is chosen randomly on the mesh and thanks to the connectivity table, we can extract the branch containing this chosen triangle. The rest of the geometry and thus the remaining triangles of the mesh will be assigned to the second branch.

- Application of the path generation method:

Our toolpath strategy is again computed, according to the topology of the part, on the three branches that have been extracted in order to obtain the toolpath on each of them. After this step, we have once again the temperature information on each of these opened or closed geometries which allows us to move on to

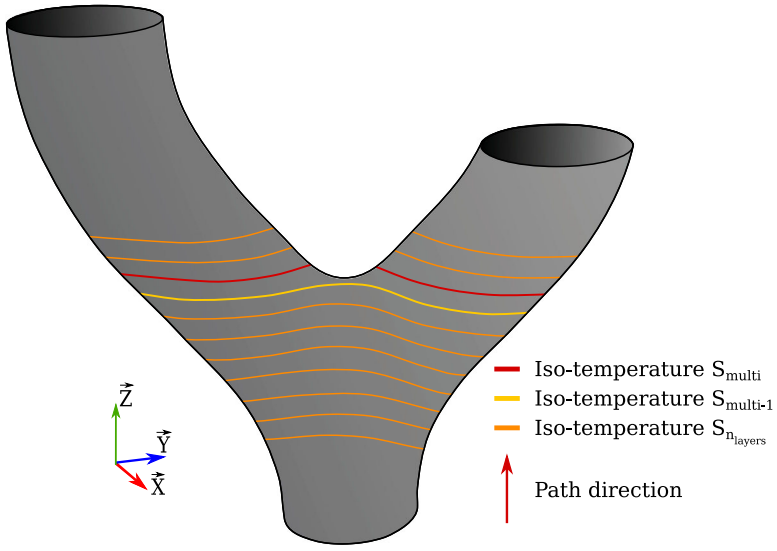

Fig. 8. Search for the detection contour of a multi-branch.

the step of "Detecting a multi-branch", in order to loop through each of the branches entirely, from the bottom to the top.

- Detecting a multi-branch:

This step is repeated to check if one of the two extracted branches is a multi-branch. If it is, this process must be repeated until all branches have been traversed and all paths have been created as described in the pseudo-code 1.

2.8. Robot orientation during manufacturing and height discontinuity of the deposit

To finalize this strategy of continuous toolpath in 3D, it is necessary to determine the orientation of the welding nozzle thanks to a Frenet reference frame. This mark will allow the torch to be oriented along its path to correspond to a 6-axis manufacturing strategy by ensuring a surface quality without step effects. The reference is defined at each point by the normal to the surface $\vec{n}$, the tangent vector $\vec{t}$ and the direction of construction $\vec{b}$ at each point is defined by the result of the calculation of the vector product between $\vec{n}$ and $\vec{t}$. It is possible to know the real deposit H_{real}, at each point during the manufacturing process, by projecting d_i, with $i \in [1, n_{pts}]$ is the number of points on the iso-contour, on the construction direction $\vec{b}$, as shown in Fig. 9. The real deposition height is given by Eq. (6).

$$H_{real} = \{H_{1,1}, \ldots, H_{n_{pts},n_{layers}}\} \tag{6}$$

where :

$$H_{1,1} = d_1 \times cos(\theta_{1,1})$$
$$H_{n_{pts},n_{layers}} = d_1 \times cos(\theta_{n_{pts},n_{layers}})$$

Initially, the spiral trajectory must be initialized and perform its first revolution where the height of the deposit of material varies linearly between h_{min} and h_{max}. However, during the second revolution, a discontinuity is created, because the deposit during the initiation of the weld bead does not have a zero height and the deposit interval $[h_{min}, h_{max}]$ limits the modulation of the latter (Fig. 10(b)).

Propagation and accentuation during subsequent layers must be eliminated, so the implementation of a deposition height control strategy. h is the average deposition height at each revolution j and Δh_j the difference between the maximum and minimum height reached during this same revolution j as represented in Fig. 10(a). At each revolution, $\Delta h_j = j * (h_{max} - h_{min})$ increases, which leads to a phenomenon of jumping between the different layers. To solve this problem, the created Z points (Section 2.6) are calculated, thanks to the strategy explained in the previous section, according to a linear distribution between h_{min} and h_{max}. The result is a layer with a regular deposit on which the discontinuity has been eliminated [42].

3. Application of toolpath strategy

The continuous trajectory generation method is implemented on PYTHON and C++. Two Open Source libraries are used, the first one is "The Computational Geometry Algorithms Library" (CGAL) [43] which is a software project that gives access to simple and efficient geometric algorithms. It is used in fields working with geometry such as computer-aided design and robotics. It will be used for geodesic distance calculation to determine the optimal closure point and the number of level layers. The second library "The Visualization Toolkit" (VTK) [41] is a scientific data visualization and manipulation software. It will be used to create temperature mapping, iso-temperatures, and continuous path visualization. After developing our algorithm, its validation is presented through the realization of three parts, one opened, one closed and one opened multi-branch part in the following section.

3.1. Opened parts

The chosen opened part, shown in Fig. 1(a), is a geometry with several curvatures and a non-planar top free edge to exploit the benefits of strategy to the fullest. The geometry has no symmetry plan to add an additional constraint to the application of the method, but also manufacturing constraints. The base was also chosen so that it is not perpendicular with the substrate which brings an additional challenge for the application of the method. All these requirements were chosen in order to show the performance of the thermal scalar field as opposed to a geodesic distance field. The use of geodesic distances does not allow the correct treatment of open geometries whose upper free edge is not flat and not perpendicular to the manufacturing direction. Indeed, in the case of open parts, the boundary conditions that erase the influence of the free edges are problematic. This is why the thermal scalar field strategy allowed to take into account the

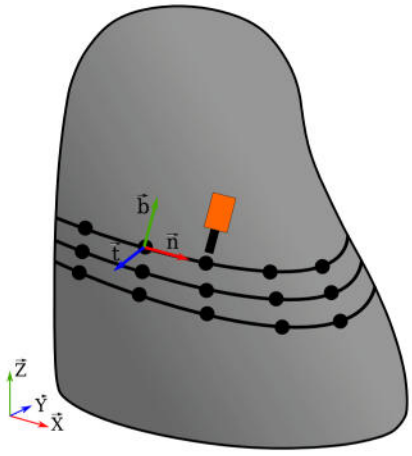

(a) Orientation of the welding torch with the Frenet coordinate system at each point.

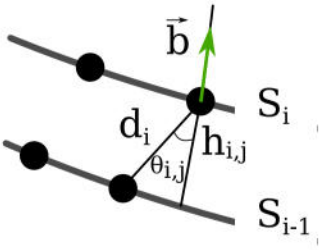

(b) Calculation of the real deposit height.

Fig. 9. Elimination of the discontinuity induced by the deposition of the first layers of the toolpath.

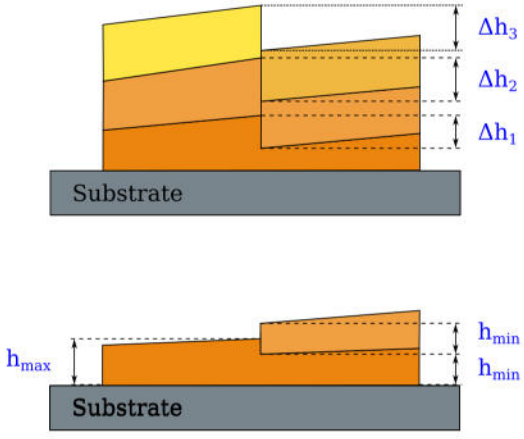

(a) Discontinuity of deposition height at the beginning of the second layer.

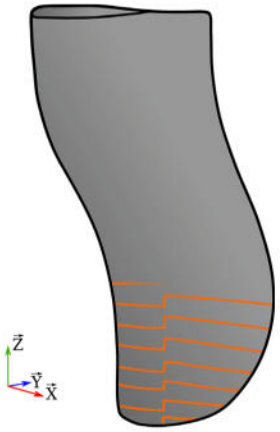

(b) Discontinuity of the trajectory that creates a "stairs effect".

Fig. 10. Elimination of the discontinuity induced by the deposition of the first layers of the toolpath.

Table 1
Parameters used for opened part presented in Fig. 11(b).

Average deposit h	2.0 mm
Minimum deposit h_{min}	1.8 mm
Maximum deposit h_{max}	2.2 mm
Minimum geodesic distance	152 mm
Maximum geodesic distance	178 mm
Number of layers	84
Number of paths	1

constraints of the free edges as shown in Fig. 11(a) as opposed to Fig. 11(b).

The parameters that have been calculated with the application of the Thermal Scalar Field for Continuous Toolpath are presented in the Table 1.

The variation of the deposit height is acceptable considering the material available for the realization of the part (see Section 4.1). The creation of the temperature gradient mapping on the opened part gives an information of the latter on all the nodes of the Ω mesh. The temperature parameters are as follows: the temperature T_{lower} is set to 20 °C and the temperature T_{upper} is set to 1000 °C. They have been chosen in an arbitrary way by respecting the condition $T_{lower} < T_{upper}$. The scalar temperature field is represented in Fig. 11(b) as well as the 84 iso-temperatures resulting from this analysis. Following these two steps, is generated the continuous spiral path as explained in Section 2.6.

After the application of this method the continuous trajectory is obtained as illustrated in Fig. 12. The manufacturing will be done along this trajectory with an average deposit of 2 mm ± 10%, including the modulation of deposit allowed by the technology used for this study are detailed in Section 4.1.

3.2. Closed parts

The closed part chosen for validation is a geometry with a single plane of symmetry (Oxz) which is shown in Fig. 1(b). This shape has a variable section with variations in curvature. Applying the strategy for closed parts, first implies the determination of the optimal point of closure.

The optimal closure point is searched using the method described in Section 2.3. With our "Elephant's foot" shape, this point is at the coordinates $(-40.47, -1.05, 258.64)$ as represented in Fig. 13. The point belongs to the plane of symmetry (Oxz) but

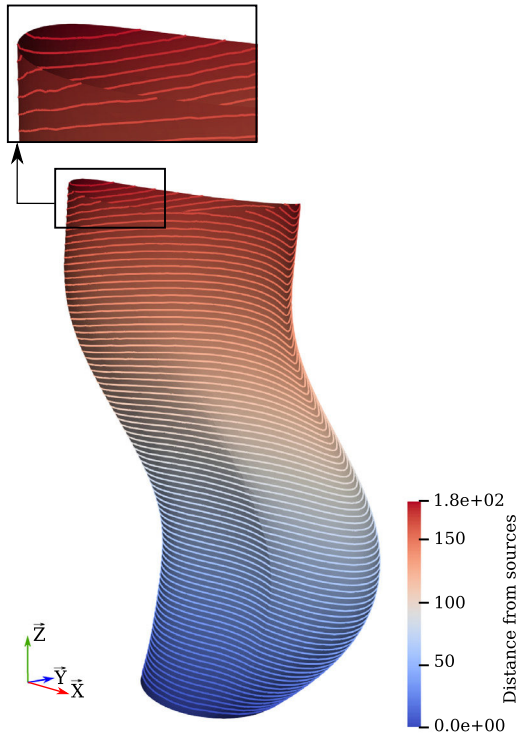

(a) Extraction of iso-values from a geodesic distance field.

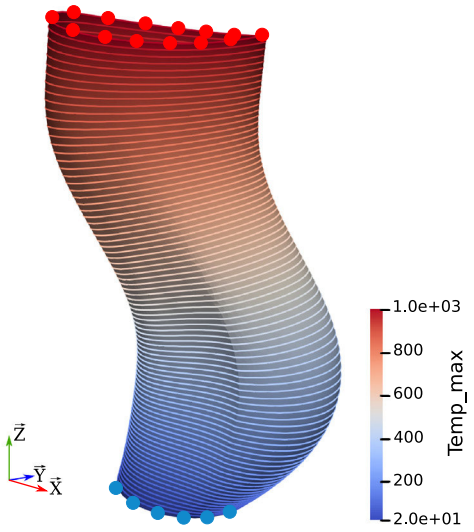

(b) Extraction of iso values from a thermal scalar field from the application of the Thermal Scalar Field for Continuous Toolpath.

Fig. 11. Comparison of iso-values not taking into account the free edge (Fig. 11(a)) and iso-values constrained by the free edge (Fig. 11(b)).

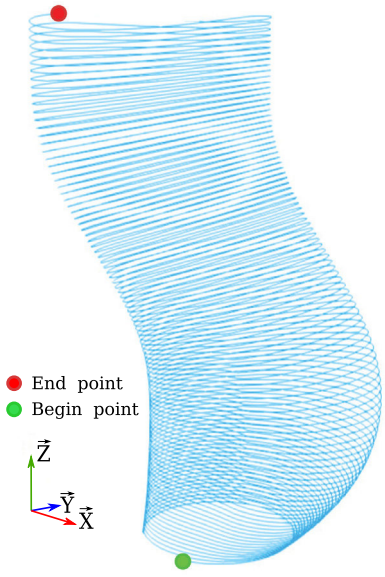

Fig. 12. Continuous three-dimensional path obtained with Thermal Scalar Field for Continuous Toolpath to manufacture the opened part.

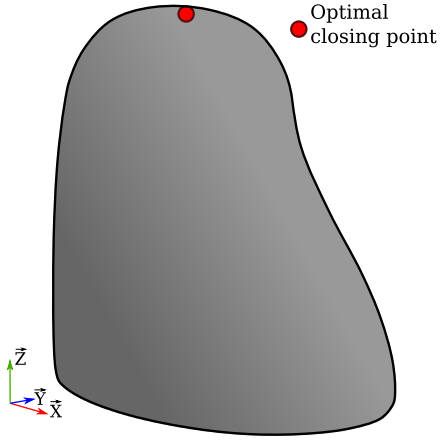

Fig. 13. Optimal closing point of "Elephant's foot" part.

Table 2
Parameters used for closed part presented in Fig. 14.

Average deposit h	2.0 mm
Minimum deposit h_{min}	1.8 mm
Maximum deposit h_{max}	2.2 mm
Minimum geodesic distance	303 mm
Maximum geodesic distance	323 mm
Number of layers	168
Number of paths	1

is not exactly at the top of the geometry because of its slender shape. After obtaining the optimal point of closure, the generation of toolpath is applied. The parameters that have been used and calculated are summarized in Table 2.

The application of the "Thermal Scalar Field for Continuous Toolpath" gives us the mapping of the temperature propagation, between the free edge $\partial\Omega_{lower}$ and the nodes belonging to the upper free edge $\partial\Omega_{upper}$. The temperature T_{lower} is fixed at 20 °C for the lower free edge while the temperature T_{upper} is fixed at 1000 °C for the upper free edge, in the same way as the opened part. The heat propagation can be seen in Fig. 14.

The continuous manufacturing path is generated on the closed part in the same way as for the opened part thanks to the iso-temperatures calculated previously, see Section 2.6, as we can see in Fig. 14. The material deposition will be done along the toolpath,

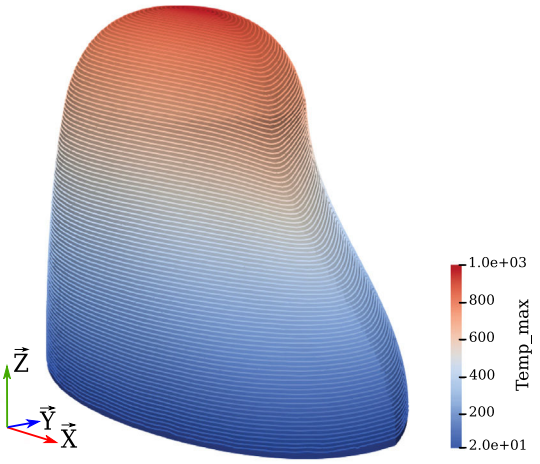

Fig. 14. Temperature mapping and iso-temperature of closed part "Elephant's foot".

Table 3
Parameters used for multi-branch part presented.

Average deposit h	2.0 mm
Minimum deposit h_{min}	1.8 mm
Maximum deposit h_{max}	2.2 mm
Maximum geodesic distance	370 mm
Number of layers	205
Number of paths	16

with an average deposition of 2 mm and a modulation ± 10% imposed by the robot used.

3.3. Multi-branch parts

The multi-branch part chosen for validation is an opened geometry from topological optimization. This free-form shape allows to show the versatility of the segmentation method but also of the toolpath strategy. The application of this method was done independently on each of the 22 branches that were found following the cutting of the shape into simple elements. We obtain the mapping of the temperature propagation of the latter (Fig. 15), between the free edge $\partial\Omega_{lower}$ and the nodes belonging to the upper free edge $\partial\Omega_{upper}$. The temperature T_{lower} is set to 20 °C for the lower free edge while the temperature T_{upper} is set to 1000 °C for the upper free edge, on each of the different branches, as for the opened and closed part. The parameters that were used and calculated after the segmentation of the multi-branch part are summarized in Table 3.

The continuous path is generated on the multi-branch part in the same way as for the opened part thanks to the iso-temperatures calculated previously, see Section 2.6. However, in the case of a multi-branch part, we obtain a continuous path for each branch, which corresponds to 16 toolpaths (see Fig. 16).

4. Experimental validation

In this part, the experimental validation of the method is done by manufacturing and measuring the two parts presented previously (Figs. 1(a)–1(b)). The first one, the closed part will be used for the validation of the parts of closed type and the second one, the one called "Elephant's trunk" for the parts named as opened. The closed part presents additional constraints contrary to the opened part. Indeed, the spiral trajectory tightens at the level of what is called the closing zone. In this area, a first collision

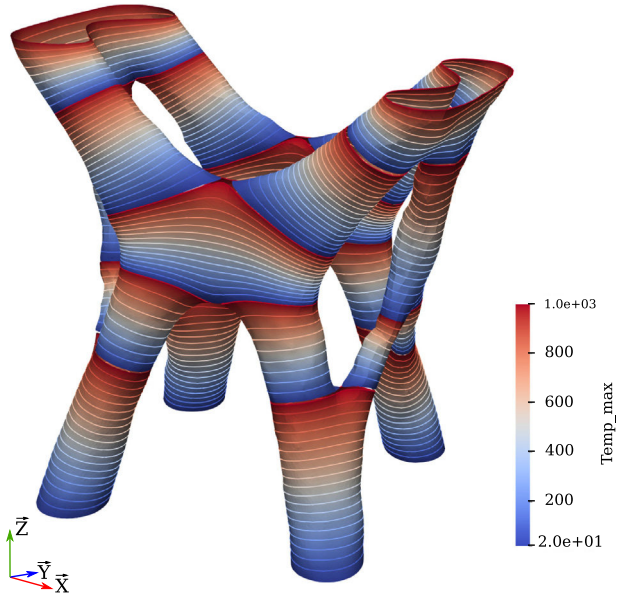

Fig. 15. Extraction of the different parts of the open multi-branch part from topological optimization and application of the Thermal Scalar Field for Continuous Toolpath on each of the branches.

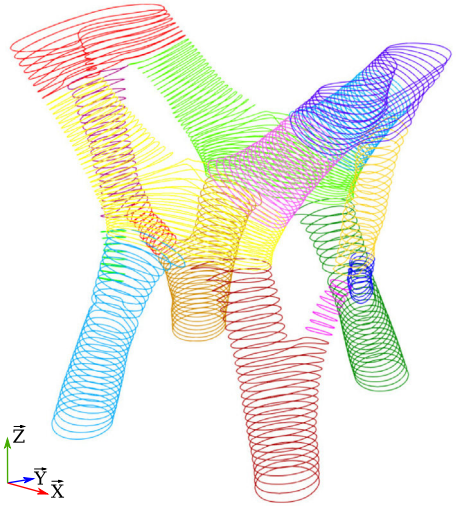

Fig. 16. Continuous three-dimensional trajectory obtained by Thermal Scalar Field for Continuous Toolpath and the segmentation method to fabricate the open multi-branch part from the topological optimization. Each of the 16 colors represents a continuous trajectory. (For interpretation of the references to color in this figure legend, the reader is referred to the web version of this article.)

problem can occur between the welding nozzle and the workpiece. Therefore, it is important to set up a nozzle reorientation algorithm to avoid this problem, which is only related to the manufacturing process. The welding process, whatever its type, has limitations due to the use of the manufacturing method with continuous trajectories. The purpose of this method is not to have stops of the weld bead, which means that no cooling period can take place during the manufacturing process and can cause overheating at these points. The size of the melt pool and the overheating causes the material to collapse, as the temperature of the part approaches the melting temperature of the steel used and the melt does not have time to solidify quickly enough. A solution that could be considered would be to make a pause

Fig. 17. The system used to manufacture the parts consists in a KUKA robotic arm equipped with a CMT welding torch.

in the overheating zones to allow the part to cool down [15], but this would lose the interest of the continuous trajectory. Varying the parameters related to the welding process, presented in Section 4.2, is more relevant.

4.1. Materials

For the production of these parts, the system consists of a 6-axis KUKA KR 16 R1610-2 [44] robotic arm, as shown in (Fig. 17) , which allows for an increased production range thanks to a large working area and freedom of movement. The robot is controlled by the KUKA control software coupled with an XML Ethernet module during production, which allows the management of welding speed, wire supply and the position of the production points in real time. The welding system is based on cold metal transfer, which has the advantage of reducing the temperature of the molten pool and the formation of splatter. It is of the GMAW type and is mechanically controlled to manage the melting of the metal and its deposit. The articulated arm is used with welding torch developed by Fronius [45], with its 6 degrees of freedom including 3 translations (X, Y, Z) and 3 rotations (Rx, Ry, Rz) linked to a Cartesian frame of reference which allows to have a coaxial transfer of energy and matter. A turntable is installed on the execution unit allowing a total number of degrees of freedom of 9 : the first 6 degrees of freedom thanks to the robot and 3 more using the turntable. The figure shows the robot equipped with the Fronius CMT welding torch which the individual parts were manufactured with. However, the parts were manufactured using only the 6 degrees of freedom of the robot.

The reproducibility of the positioning is far better that the repeatability of the deposition. The position is given incrementally by the supervision software along the serial port of the robot

Table 4
Different properties of the steel G3Si used and of the thermal Scalar Field for Continuous Toolpath.

Volumetric mass	7800 kg/m^3
Melt temperature	1700 K
Thermal diffusivity	14e^{-6}m^2/s
Surface tension in Argon	1.6 N/mm
Diameter Torch	24 mm
Diameter wire	1 mm
Wire feed velocity	2 m/min
Welding time	1.5 s

controller. A library sends the instructions and verifies that it was received (or done) by the robot. The work pieces are all manufactured in the center of the workspace of the robot to prevent any kinematic singularities. The metal used is G3Si steel and the shielding gas composed of 92% Argon and 8% CO2 is directed directly with the welding torch. Table 4 summarizes some properties of the steel used as well as the parameters specific to our method of generating toolpaths for the realization of the two parts. The substrate used will be a 6 mm thick G3Si steel plate of variable dimensions depending on the size of the part.

4.2. Manufacturing part

The WAAM process allows the modulation of the deposition height by varying given parameters. With this method, it is possible to control the wire feed speed *WFS*, the welding time *TS*, the width *BW* and the height *BH* of the weld bead. But also the power of the heat source by acting on the voltage *U* and the intensity *I*. For the manufacturing of the parts, the welding speed *WS* is constant. A relation Eq. (7) [19] can be established allowing to obtain the desired deposition height on each stratum according to the various proceeding parameters. In addition, to establish this relation, the assumption that the section of the weld beam deposited is circular is adopted.

$$BH = \frac{\pi \times d_w^2 \times WFS}{4 \times BW \times TS} \tag{7}$$

The parts are manufactured in steel using the WAAM process and are presented in Figs. 18(a) and 18(b). A complex multi-branch part resulting from topological optimization has been fabricated in order to demonstrate the versatility of the method (Fig. 18(c)). Only one start/stop phase, thus only one weld bead, was necessary to manufacture the single-branch parts, which means that the trajectory is continuous. The multi-branch part, being a multi-branch part, was made in 22 continuous beads which corresponds to the number of branches resulting from the segmentation of this geometry. Compared to a classical 2.5D strategy, this allowed to reduce the manufacturing time by avoiding the start/stop phases where it is necessary to let the part cool down.

With a strategy 2.5D, at each change of layer, it is necessary to wait a given time to avoid the problem related to the previous layers which already heated the part. These overheating cause problems of distortion of the part, but also, a reduction of the surface state related to collapses of material due to a temperature of the part too high. These collapses occur when the part temperature approaches the melt temperature. With the presented continuous path method, the problem of waiting time between layers is eliminated. The manufacturing time is greatly reduced and allows for a superior manufacturing quality. To illustrate this point we will take the example of the “Elephant’s trunk” part which was manufactured in 84 revolutions. In a 2.5D strategy, an inter-layer cooling time is often necessary to cool the part.

(a) Manufacturing opened part "Elephant's trunk" with an average deposit of 2mm.

(b) Manufacturing closed part called "Elephant's foot" with an average deposit of 2mm.

(c) Manufacturing of a multi-branch part from topological optimization with an average deposit of 2mm.

Fig. 18. Parts manufactured with our algorithm and the segmentation method for the multi-branch part.

Assuming that an inter-layer cooling time would be necessary in the fabrication of the "Elephant's trunk" part, we can quickly realize that a continuous fabrication strategy. We can choose an inter-layer cooling time equal to 1 min which increases the manufacturing time of this part by 1 h and 24 min. With an initial manufacturing time of 50 min, the 2.5D strategy allows the part to be manufactured in approximately 2 h and 14 min, an increase of 168%. The manufacturing process does not require the use of supports thanks to its versatility linked to its 5-axis strategy. We can also notice that the parts do not present any staircase effect, an effect that is often present with cutting strategies in 2.5D. The opened part in Fig. 18(a) required 84 revolutions to complete this part in 50 min with an average deposit of 2 mm. One of the particularities of the "Elephant's trunk" is its non-planar upper free edge. Indeed, this shows the limits of the manufacturing methods in 2.5D which cannot realize trajectories out of their own plane. It is therefore impossible to finish a non-planar geometry at its end with this kind of strategies. As for the closed part shown in Fig. 18(b), measuring 250 mm in height, it was manufactured in about 1 h and 30 min with 168 revolutions and an average material deposit of 2 mm. The manufacturing of several parts with a variable weld bead diameter allowed to realize that this parameter is directly linked to the surface quality of the part and therefore to reduce the deviation between the CAD and the manufactured part.

4.3. Feasibility criterion

The limitation of the modulation range of the deposit height imposed by the tooling used is a limit to the realization of free-form parts with a continuous toolpath. The equipment used for the validation in the present paper allows a modulation of deposit of $\pm$ 10%. With a higher variation, it is possible to realize even more complex parts. To allow a deposit in the modulation range during the whole manufacturing of the geometry, it is necessary that the part meets the criteria given by Eq. (8).

$$max(H_{real}) \leq h_{max} \quad and \quad min(H_{real}) \leq h_{min} \tag{8}$$

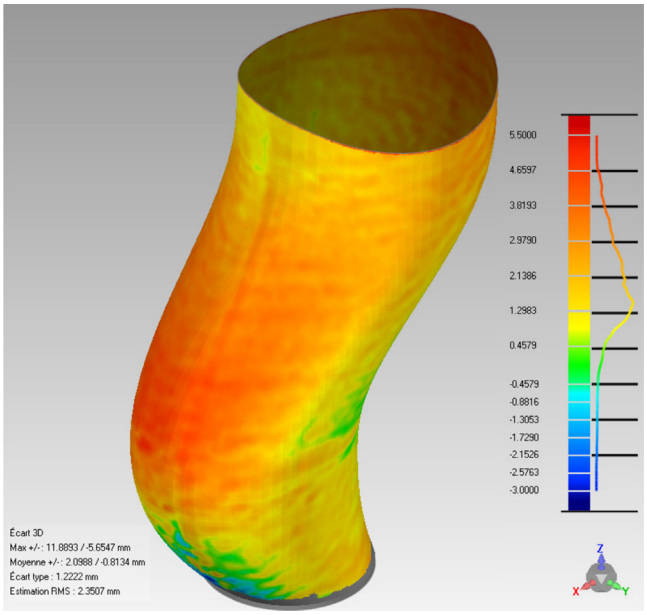

Fig. 19. Comparison between the surface from the scan and the CAD of "Elephant's trunk".

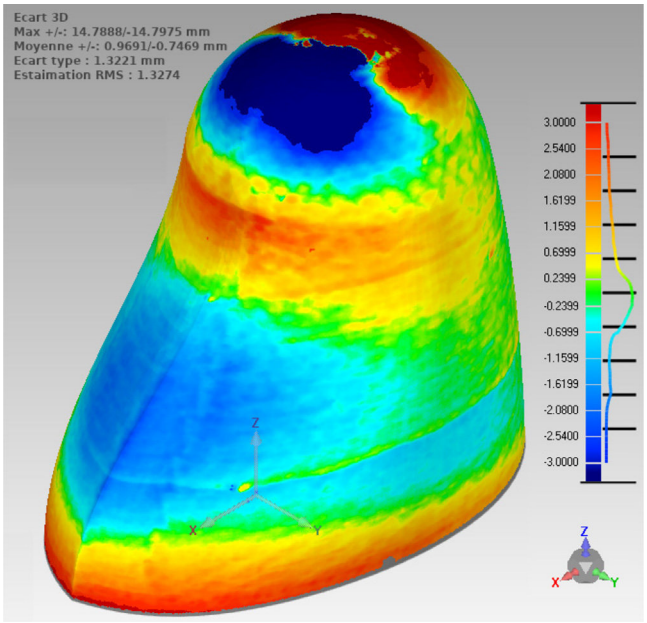

Fig. 20. Comparison between the surface from the scan and the CAD of closed part.

This criterion influences the complexity of the structures that can be fabricated with this method. The feasibility depends on the control of the manufacturing process parameters that vary the deposition height. The greater the modulation range, the more complex the parts produced can be. This criterion makes it possible to evaluate upstream if any geometry can be manufactured with a continuous trajectory and thus limits the study of the latter if it does not respect it.

4.4. Comparison between CAD and manufactured parts

To validate our strategy operating on these two types of structures, a comparison between the CAD and the manufactured part and thus its reproducibility fidelity. The parts have been scanned using a Creaform MetraSCAN3D scanner [46]. This laser scanner calculates the point cloud extracted from the manufactured part. Using GEOMAGIC software [47], a global registration (ICP algorithm) and a 3D map deviation between the mesh of the scan and the CAD are performed. The file resulting from the scan is then recalibrated thanks to the substrate in relation to the normal of the latter. After this step, the GEOMAGIC software [47] is used to compare the STL file and the manufactured part (see Figs. 19 and 20).

With a more detailed study thanks to the analysis which allowed the comparison of the part with the CAD, an average deviation ranging between [−0.813 mm, 2.099 mm] for the opened part is calculated (see Fig. 19). We notice that the part does not present any staircase effect (Section 1.1) and a very satisfactory surface condition in its globality. Some areas have more important deviations from the CAD. These deviations are due to the important tilt of the geometry, near its base, where collapses were starting appearing in this area. It is possible to reduce this phenomenon by making the part with an average deposit lower than the 2 mm chosen which will increase the accuracy of the restitution of the part in its entirety.

Concerning the part named "Elephant's trunk", the average deviation is 0.8 mm with a range between [−0.747 mm, 0.969 mm] (see Fig. 20) with a good surface finish without step effect. A lower deviation is obtained for this part, because the melt is not subjected to gravity unlike the opened part.

5. Conclusion

WAAM is a technology with great potential, but it is still limited by the use of 2.5D path generation strategies that cannot realize complex structures without many start/stop phases giving poor surface finish. In order to manufacture parts with geometrical peculiarities, excluding 2.5D methods, such as non-planar upper free edges, curvature variations, and even closed parts, it was necessary to develop a 3D trajectory planning strategy. The method presented in this paper takes advantage of previously unexploited benefits of WAAM, such as the use of multi-axis machines to perform multi-axis printing and the modulation of weld bead height. This 3D continuous path generation strategy, called "Thermal Scalar Field for Continuous Toolpath", is applied to thin free-form parts. It is based on a curvilinear cutting of a part thanks to a thermal scalar field calculated by finite elements in order to create a thermal map of the part and thus create iso-temperatures. Iso-temperatures are chosen to fit an average thickness of deposit directly linked to the technology used. They are then discretized into the same number of points that are connected to create the continuous path. This strategy differs according to the type of parts to be produced which are identified as opened parts, closed parts and even so-called multi-branch parts. In the case of a closed part, it is necessary to determine the optimal closing point that will act as the upper free edge to apply this strategy unlike opened parts. For multi-branch parts, the continuous strategy is not possible. However, we can segment these parts to create pseudo-continuous trajectories. The method was also validated by printing in WAAM the three parts (Figs. 21 and 18(c)) with a continuous trajectory using only one start/stop phase of the arc.

The elimination of these start/stop phases reduces the manufacturing time and the heat input related to these phases, which are typical of 2.5D strategies. In a second step, a comparison between the surfaces of the CAD part and the part after manufacturing is performed by evaluating the deviations using a scan of the manufactured part. The perspective related to this method would be to manage the collapse of the structure during the closing of a closed part. Thermal modeling of these areas could be

Fig. 21. Three parts manufactured with our Thermal Scalar Field for Continuous Toolpath.

done to have additional information on necessary waiting times or reduction of the welding speed to cool these areas during manufacturing process and avoid their collapse.

CRediT authorship contribution statement

A. Giordano: Software, Formal analysis, Writing – original draft, Writing – review & editing, Visualization. **A. Diourté:** Conceptualization, Methodology, Formal analysis, Writing – review & editing. **C. Bordreuil:** Validation, Investigation, Writing – review & editing. **F. Bugarin:** Conceptualization, Methodology, Software. **S. Segonds:** Conceptualization, Methodology, Software.

Declaration of competing interest

The authors declare that they have no known competing financial interests or personal relationships that could have appeared to influence the work reported in this paper.

References

[1] Williams SW, Martina F, Addison AC, Ding J, Pardal G, Colegrove P. Wire + arc additive manufacturing. Mater Sci Technol 2016;32(7):641–7.

[2] Chu Won-Shik, Kim Chung-Soo, Lee Hyun-Taek, Choi Jung-Oh, Park Jae-Il, Song Ji-Hyeon, Jang Ki-Hwan, Ahn Sung-Hoon. Hybrid manufacturing in micro/nano scale: A review. Int J Precis Eng Manuf-Green Technol 2014;1(1):75–92.

[3] Ding J, Colegrove P, Mehnen J, Ganguly S, Sequeira Almeida PM, Wang F, Williams S. Thermo-mechanical analysis of Wire and Arc Additive Layer Manufacturing process on large multi-layer parts. Comput Mater Sci 2011. S092702561100365X.

[4] Li Rong, Xiong Jun, Lei Yangyang. Investigation on thermal stress evolution induced by wire and arc additive manufacturing for circular thin-walled parts. J Manuf Process 2019;40:59–67.

[5] Ding Donghong, Pan Zengxi, Cuiuri Dominic, Li Huijun. A tool-path generation strategy for wire and arc additive manufacturing. Int J Adv Manuf Technol 2014;73(1–4):173–83.

[6] Diourté Adama, Bugarin Florian, Bordreuil Cyril, Segonds Stéphane. Continuous three-dimensional path planning (CTPP) for complex thin parts with wire arc additive manufacturing. Addit Manuf 2021;37:101622.

[7] Ma Weiyin, But Wing-Chung, He Peiren. NURBS-based adaptive slicing for efficient rapid prototyping. Comput Aided Des 2004;36(13):1309–25.

[8] Ding Donghong, Pan Zengxi, Cuiuri Dominic, Li Huijun. A practical path planning methodology for wire and arc additive manufacturing of thin-walled structures. Robot Comput-Integr Manuf 2015;34:8–19.

[9] Venturini Giuseppe, Montevecchi Filippo, Bandini Francesco, Scippa Antonio, Campatelli Gianni. Feature based three axes computer aided manufacturing software for wire arc additive manufacturing dedicated to thin walled components. Addit Manuf 2018;22:643–57.

[10] van Sosin Boris, Rodin Daniil, Sliusarenko Hanna, Bartoň Michael, Elber Gershon. The construction of conforming-to-shape truss lattice structures via 3D sphere packing. Comput Aided Des 2021;132:102962.

[11] Zhang YuMing, Chen Yiwei, Li Pengjiu, Male Alan T. Weld deposition-based rapid prototyping: a preliminary study. J Mater Process Technol 2003;135(2–3):347–57.

[12] Ding Donghong, Shen Chen, Pan Zengxi, Cuiuri Dominic, Li Huijun, Larkin Nathan, van Duin Stephen. Towards an automated robotic arc-welding-based additive manufacturing system from CAD to finished part. Comput Aided Des 2016;73:66–75.

[13] Kwak Yong-Min, Doumanidis Charalabos C. Geometry regulation of material deposition in near-net shape manufacturing by thermally scanned welding. J Manuf Process 2002;4(1):28–41.

[14] Wang Yiming, Xu Xingwang, Zhao Zhuang, Deng Wenxiang, Han Jing, Bai Lianfa, Liang Xianglong, Yao Jianyong. Coordinated monitoring and control method of deposited layer width and reinforcement in WAAM process. J Manuf Process 2021;71:306–16.

[15] Montevecchi Filippo, Venturini Giuseppe, Grossi Niccolò, Scippa Antonio, Campatelli Gianni. Idle time selection for wire-arc additive manufacturing: A finite element-based technique. Addit Manuf 2018;21:479–86.
[16] Kazanas Panagiotis, Deherkar Preetam, Almeida Pedro, Lockett Helen, Williams Stewart. Fabrication of geometrical features using wire and arc additive manufacture. Proc Inst Mech Eng B 2012;226(6):1042–51.
[17] Mehnen Jörn, Ding Jialuo, Lockett Helen, Kazanas Panos. Design study for wire and arc additive manufacture. Int J Prod Dev 2014;19(1/2/3):2.
[18] Etienne Jimmy, Ray Nicolas, Panozzo Daniele, Hornus Samuel, Wang Charlie CL, Martí nez Jonàs, McMains Sara, Alexa Marc, Wyvill Brian, Lefebvre Sylvain. CurviSlicer: slightly curved slicing for 3-axis printers. ACM Trans Graph 2019;38(4):1–11.
[19] Hascoët Jean-Yves, Querard Vincent, Rauch Matthieu. Interests of 5 axis toolpaths generation for wire arc additive manufacturing of aluminum alloys. J Mach Eng 2017;17(3):15.
[20] Ezair Ben, Massarwi Fady, Elber Gershon. Orientation analysis of 3D objects toward minimal support volume in 3D-printing. Comput Graph 2015;51:117–24.
[21] Liu Xiuping, Lin Liping, Wu Jun, Wang Weiming, Yin Baocai, Wang Charlie CL. Generating sparse self-supporting wireframe models for 3D printing using mesh simplification. Graph Models 2018;98:14–23.
[22] Huang Yijiang, Zhang Juyong, Hu Xin, Song Guoxian, Liu Zhongyuan, Yu Lei, Liu Ligang. FrameFab: robotic fabrication of frame shapes. ACM Trans Graph 2016;35(6):1–11.
[23] Dai Chengkai, Wang Charlie CL, Wu Chenming, Lefebvre Sylvain, Fang Guoxin, Liu Yong-Jin. Support-free volume printing by multi-axis motion. ACM Trans Graph 2018;37(4):1–14.
[24] Wu Chenming, Dai Chengkai, Fang Guoxin, Liu Yong-Jin, Wang Charlie CL. RoboFDM: A Robotic system for support-free fabrication using FDM. In: 2017 IEEE international conference on robotics and automation (ICRA). Singapore, Singapore: IEEE; 2017, p. 1175–80.
[25] Fang Guoxin, Zhang Tianyu, Zhong Sikai, Chen Xiangjia, Zhong Zichun, Wang Charlie CL. Reinforced FDM: multi-axis filament alignment with controlled anisotropic strength. ACM Trans Graph 2020;39(6):1–15.
[26] Hergel Jean, Hinz Kevin, Lefebvre Sylvain, Thomaszewski Bernhard. Extrusion-based ceramics printing with strictly-continuous deposition. ACM Trans Graph 2019;38(6):1–11.
[27] Held Martin, Spielberger Christian. A smooth spiral tool path for high speed machining of 2D pockets. Comput Aided Des 2009;41(7):539–50.
[28] Wang Yu, Yu Kai-Min, Wang Charlie CL. Spiral and conformal cooling in plastic injection molding. Comput Aided Des 2015;63:1–11.
[29] Xu Ke, Li Yingguang, Chen Lufeng, Tang Kai. Curved layer based process planning for multi-axis volume printing of freeform parts. Comput Aided Des 2019;114:51–63.
[30] Radel S, Diourte A, Soulié F, Company O, Bordreuil C. Skeleton arc additive manufacturing with closed loop control. Addit Manuf 2019;26:106–16.
[31] Yili Dai, Shengfu Yu, Yusheng Shi, Tianying He, Lichao Zhang. Wire and arc additive manufacture of high-building multi-directional pipe joint. Int J Adv Manuf Technol 2018;96(5–8):2389–96.
[32] Roy Souvik, Juha Mario, Shephard Mark S, Maniatty Antoinette M. Heat transfer model and finite element formulation for simulation of selective laser melting. Comput Mech 2018;62(3):273–84.
[33] Crane Keenan, Weischedel Clarisse, Wardetzky Max. The heat method for distance computation. Commun ACM 2017;60(11):90–9.
[34] Cornea Nicu D, Silver Deborah, Min Patrick. Curve-skeleton properties, applications, and algorithms. IEEE Trans Vis Comput Graphics 2007;13(3):530–48.
[35] Van Uitert Robert, Bitter Ingmar. Subvoxel precise skeletons of volumetric data based on fast marching methods: Subvoxel precise skeletons of volumetric data. Med Phys 2007;34(2):627–38.
[36] Arcelli C, di Baja Gabriella Sanniti, Serino L. Distance-driven skeletonization in voxel images. IEEE Trans Pattern Anal Mach Intell 2011;33(4):709–20.
[37] Ogniewicz RL, Kübler O. Hierarchic Voronoi skeletons. Pattern Recognit 1995;28(3):343–59.
[38] Näf M, Székely G, Kikinis R, Shenton ME, Kübler O. 3D Voronoi skeletons and their usage for the characterization and recognition of 3D organ shape. Comput Vis Image Underst 1997;66(2):147–61.
[39] Lee TC, Kashyap RL. Building skeleton models via 3-D medial surface_axis thinning algorithms. Graph Models Image Process 1994;56(6):462–78.
[40] Jin Xun, Kim Jongweon. A 3D skeletonization algorithm for 3D mesh models using a partial parallel 3D thinning algorithm and 3D skeleton correcting algorithm. Appl Sci 2017;7(2):139.
[41] Kitware ∼Inc. The Visualization Toolkit (VTK); 2014. URL https://vtk.org/.
[42] Diourte Adama. Génération et optimisation de trajectoire dans la fabrication additive par soudage à l'arc [Ph.D. thesis], Université Paul Sabatier Toulouse 3; 2021.
[43] The CGALProject. The computational geometry algorithms library. 1995.
[44] Kuka Roboter GmbH. KUKA – Robot Industriels, URL https://www.kuka.com/fr-fr/produits-et-prestations/syst%C3%A8mes-de-robots/robots-industriels/kr-cybertech.
[45] Fronius. CMT – Process de soudage – Techniques de soudage, URL https://www.fronius.com/fr-fr/france/techniques-de-soudage/univers-du-soudage/fronius-welding-processes/cmt.
[46] Creaform. MetraSCAN 3D – MMT Optique, URL https://www.creaform3d.com/fr/solutions-de-metrologie/scanners-sur-mmt-optique-metrascan-3d?aw_campaign=90.1.0-Search-Branded-France-FR&aw_campaignId=1777809807&aw_adgroupId=71811673671&aw_network=g&aw_device=c&aw_geo_location=9055242&aw_int_location=&aw_keyword=metrascan&kw=metrascan&cpn=1777809807&gclid=EAIaIQobChMI-MvB6_zS8AIVJ0iRBR01HAdOEAAYASAAEgL7bfD_BwE.
[47] 3D SYSTEMS. Geomagic Control X, 3D SYSTEMS, URL https://www.danielgm.net/cc/.